Stereodynamical Control of Nonadiabatic Quenching Dynamics of $OH(A^2S^+)$ by H_2: Full-Dimensional Quantum Dynamics

Bin Zhao
Bielefeld University https://orcid.org/0000-0001-5862-7402
Shanyu Han
University of New Mexico
Christopher Malbon
Johns Hopkins University
Uwe Manthe
Bielefeld University https://orcid.org/0000-0002-4845-9633
David Yarkony
John Hopkins University
H. Guo (hguo@unm.edu)
University of New Mexico https://orcid.org/0000-0001-9901-053X

Article

Keywords: Born-Oppenheimer approximation, stereodynamics

Posted Date: January 12th, 2021

DOI: https://doi.org/10.21203/rs.3.rs-129574/v1

Version of Record: A version of this preprint was published at Nature Chemistry on August 9th, 2021. See the published version at https://doi.org/10.1038/s41557-021-00730-1.

Abstract

The breakdown of the Born-Oppenheimer approximation is omnipresent in chemistry, but our detailed understanding of the nonadiabatic dynamics is still incomplete. In the present work, nonadiabatic quenching of electronically excited OH(A^2S^+) molecules by H_2 molecules is investigated by a full-dimensional quantum dynamical method using a high quality diabatic potential energy matrix. Good agreement with experiment is found for the OH(X^2P) ro-vibrational and L-doublet distributions. Furthermore, the nonadiabatic dynamics is shown to be controlled by stereodynamics, namely the orientation of the two reactants. The uncovering of a major (in)elastic channel, neglected in all previous analyses, resolves a long-standing experiment-theory disagreement concerning the branching ratio of the two electronic quenching channels.

1. Introduction

Although the Born-Oppenheimer (BO) approximation,[1] which assumes separability of nuclear and electronic motion, is widely accepted for characterizing reactions in their ground electronic states, there is general agreement that reaction dynamics can be significantly impacted by excited electronic states near an electronic degeneracy, where the motion of the electrons is strongly coupled with that of the nuclei. While ultrafast nonadiabatic transitions near conical intersections (CIs) have been intensively studied in photochemistry,[2–8] non-BO effects have seldom been investigated in detail for collisions and bimolecular reactions.[9] Existing first-principles theory of nonadiabatic reaction dynamics have mostly dealt with open-shell atoms, focusing on geometric phase effects[10–12] or spin-orbit excited electronic states.[13–18] In the present work, we extend the detailed first-principles theory to the collision of electronically excited molecules, namely the hydroxyl radical in the OH($A^2\Sigma^+$) state, by studying the following processes in full dimensionality:

$OH(A^2\Sigma^+) + H_2 \rightarrow H + H_2O$ (reactive quenching) (R1a)

$\rightarrow OH(X^2\Pi) + H_2$ (non-reactive quenching) (R1b)

$\rightarrow OH(A^2\Sigma^+) + H_2$ (elastic and inelastic scattering) (R1c)

Here, both non-radiative quenching channels (R1a and R1b) necessarily require transitions from a higher to lower electronic state, due to nonadiabatic couplings near degeneracies such as conical intersections (CIs).[19, 20] This system not only offers a prototype for understanding fundamental nonadiabatic dynamics in bimolecular collisions, but is also of great practical relevance to the laser-induced fluorescence (LIF) monitoring of the omnipresent OH radicals in atmospheric chemistry and in combustion.[21, 22]

Pioneering experiments by Lester and coworkers identified the reactive quenching channel (R1a)[23] and

ydrogen co-product.[24–26] These kinetic energy distributions

were found to be bimodal, suggesting complex dynamics with at least two reaction pathways. These intrabeam measurements were confirmed by a crossed molecular beam experiment by Ortiz-Suárez et al.[27] Later experiments by the Lester group investigated the nonreactive quenching channel (R1b) with quantum state resolution.[25, 28–30] The OH($X^2\Pi$) product was found to be vibrationally cold but rotationally hot. A propensity for the A' component of the OH($X^2\Pi$) Λ-doublet was also observed. Furthermore, this group reported the branching ratio between the R1a and R1b channels, which favors the former.[25] The existence of quantum state-resolved experimental data makes this system a fertile proving ground for theoretical understanding of nonadiabatic dynamics in bimolecular collisions.

Several electronic states are involved in the nonadiabatic quenching channels. In the entrance channel, the OH($A^2\Sigma^+$) + H_2 asymptote correlates adiabatically with the 3^2A state, while the doubly degenerate OH($X^2\Pi$) + H_2 asymptote correlates with the 1^2A and 2^2A states. In the reactive quenching channel, the 1^2A state correlates adiabatically with the H_2O + H asymptote. For C_s geometries, the 1^2A and 2^2A states carry irreducible representations (irreps) A" and A', while the higher 3^2A state belongs to the A' irrep. Early *ab initio* calculations identified a T-shaped (C_{2v}) CI seam between the $3^2A(^2A_1)$ and $2^2A(^2B_2)$ states, with OH pointing its O-end to H_2.[31] It was hypothesized that this CI was responsible for efficient quenching of OH($A^2\Sigma^+$), leading to both reactive and nonreactive quenching channels. Subsequent studies by Yarkony and coworkers revealed, however, that this CI seam actually spans the entire planar (C_s) geometry, extending from the C_{2v} to $C_{\infty v}$ geometries,[32, 33] where the irreps of the two states involved are A'/A', B_2/A_1, and Π/Σ, respectively. In Fig. 1(a), this confluence of the CI seam is shown as a function of the H_2-OH distance and the H_2 rotational angle, with O always pointing to H_2. This planar CI seam is responsible for nonadiabatic transitions involved in R1a and R1b, and represents the focal point of the current dynamics investigation. Further studies by Dillon and Yarkony explored the non-planar portion of the configuration space. They identified an additional CI seam between the 1^2A and 2^2A states, facilitating a non-planar insertion pathway of HO into H_2,[34, 35] leading to H and H_2O. This CI seam facilitates the population of the A' and A" Λ-doublet states of the OH($X^2\Pi$) product, and presumably also for the bimodality of the H kinetic energy distribution in the R1a channel.

Based on this electronic structure understanding, several multi-dimensional coupled potential energy surfaces (PESs) have been reported.[29, 36–40] For nonadiabatic dynamics involving more than one electronic state, it is advantageous to express the Hamiltonian in a diabatic representation[5, 41] to avoid singularities in the kinetic energy operator and cusps in the potential energy operator at the CI seams. While the resulting diabatic potential energy matrix (DPEM) is difficult to construct from adiabatic electronic structure calculations, once established, it greatly simplifies the dynamical calculations. To this end, reduced- and full-dimensional DPEMs considering two,[29, 37] three,[38, 39] and four[40] electronic states have been reported. Based on a large number of multi-reference configuration interaction calculations, the latest global DPEM offers the highest fidelity in reproducing ab initio energies of the four lowest states and their couplings.[40]

These high-quality DPEMs have opened the door for dynamical studies.[36–38, 42] While the dynamics can only be accurately characterized quantum mechanically, such calculations are challenging because of the large energy release (> 4 eV), a large accessible phase space, and the complex multi-state dynamics.[9] Until now, quantum dynamics calculations have been restricted to planar geometries with two electronic states.[37, 42] However, such a model is insufficient[38] since it neglects the 2^2A state and important non-planar dynamics. On the other hand, full-dimensional trajectory surface hopping (TSH) studies have been employed to gain insights into the quenching events, but the results had no quantum state resolution. Interestingly, the TSH results favored the nonreactive quenching channel, in sharp contrast to the experiment.[25] The R1a/R1b branching ratio is a fundamental quantity in this nonadiabatic process, the experimental/theoretical discrepancy is therefore of considerable importance. It could be due to the semi-classical treatment of the nonadiabatic dynamics and/or inaccuracies in the DPEM. This issue is thus only resolvable by a full-dimensional quantum dynamics study on a globally accurate DPEM.

In this work, we report the first full-dimensional investigation of the nonadiabatic collisional quenching of OH($A^2\Sigma^+$) by H_2 using a time-dependent quantum wave packet method on the recently developed DPEM.[40] We aim to resolve the aforementioned experiment-theory discrepancy, to validate the DPEM by comparing quantum state resolved product distributions with experiment, and to gain insight into the (stereo)dynamics of this prototypical nonadiabatic process.

2. Results

The calculated fraction for the nonreactive quenching channel (f_{R1b}) at the collision energy of 0.05 eV is 0.123, and that for reactive quenching R1a is f_{R1a} = 0.100. The former is in excellent agreement with the experimental value (0.12(5)).[25] However, our results suggest that nonreactive quenching is slightly favored over reactive quenching (R1a) at this energy. The preference to the R1b channel increases with the increasing collision energy, as the data in Table 1 show. This preference, consistent with the earlier TSH results based on a DPEM of Collins et al.,[38] is in sharp contrast to the experimental report by Dempsey et al.,[25] in which the reactive quenching channel dominates. As discussed in the next section, we attribute the experiment-theory discrepancy to the large yield of the R1c channel, which was neglected in the previous determination of the branching ratio. In the same Table, TSH results with zero impact parameter (b = 0) are also listed for comparison, and they provide a qualitatively but not quantitatively correct description of the process.

The internal state distributions of the OH($X^2\Pi$) product were calculated at the three collision energies. Figure 2 displays the OH($X^2\Pi$) ro-vibrational state-resolved probabilities for both the A' and A" components of its Λ-doublet. The present calculations showed that the OH($X^2\Pi$) products are dominantly in the ground vibrational state with a broad rotational state distribution peaking at N_{OH}=17, in good agreement with experimental observations,[28] shown in the top panels of the same figure. The peak of the distribution shifts towards higher N_{OH} with increasing collision energy. Furthermore, Lester and coworkers

reported that the OH($X^2\Pi$) products are mainly formed in the A' component of this degenerate electronic state,[28] a trend reproduced by our calculated distributions.

The H_2 ro-vibrational state distribution has also been calculated, although there are currently no experimental data to compare. In Fig. 3, the final H_2 vibrational and rotational state-resolved probabilities are displayed. The H_2 products are both vibrationally and rotationally hot, and only *ortho*-H_2 is formed. The absence of the *para*-H_2 can be attributed to the permutation symmetry of the DPEM, as discussed in more detail in the next section. The H_2 vibrational state distribution extends to higher vibrational states when the collision energy is increased.

3. Discussion

Our wave packet calculations revealed that the fate of the collision between OH($A^2\Sigma^+$) and H_2 is strongly controlled by stereodynamics, which has important consequences in the quenching process. As recognized before,[31] the OH($A^2\Sigma^+$) + H_2 entrance channel on the excited 3^2A state with the H-end of OH pointing towards H_2 () features barrierless access to a T-shaped van der Waals (vdW) well, which has a depth of 0.34 eV. The spectrum and lifetimes of predissociative states in this well have been a subject of extensive studies by Lester and coworkers.[31] However, this approach has no easy access to the CI seam because of a large barrier separating the vdW well from the upper cone of the CI, which corresponds to changing from to 0 °, as illustrated in Fig. 1(b) and in more detail in Figure S1 in Supporting Information (SI). As a result, the wave packet is largely reflected back to the OH($A^2\Sigma^+$) + H_2 channel by the repulsive wall. Noting that the O-H and H-H bond lengths in the vdW well (1.975 a.u. and 1.461 a.u.) are essentially the same as those of the free molecules, there is thus little vibrational excitation. The T-shape also dictates that rotational excitation is minimal because no torque results from momentum transfer. These features are shown in Figure S2 in SI. Importantly, this particular steric approach leads to the large R1c yield shown in Table 1, although the dominance of this (in)elastic channel is weakened at higher energies.

On the other hand, the upper cone of the 3^2A-2^2A CI can be accessed, also without a barrier as shown in Figs. 1(a) and 1(b), when OH($A^2\Sigma^+$) approaches H_2 with its O-end (). This CI seam has been identified in previous work,[32, 33] but most discussion on its effect has focused on the seam in the C_{2v} symmetry.[29, 31] Interestingly, our quantum dynamics calculation indicates that the wave packets emerging on the 1^2A and 2^2A states are largely located near the H-H-O-H collinear geometry (and), as shown in Fig. 4 (and Movie S1 and Figure S3 in SI). This observation underscores the dominance of the collinear reaction pathway over the C_{2v} pathway proposed in previous work.[29, 31] A closer examination of the CI seam revealed the origin of this behavior: The asymptote 3^2A PES has a large anisotropy with respect to the H_2 rotational angle (), as shown in Fig. 1(a) (and Figure S4 in SI), which guides the incoming wave packet to

the linear geometry. Indeed, the minimum energy crossing (MEX) with $C_{\infty v}$ symmetry is ~ 0.631 eV lower than that at C_{2v} symmetry, the C_s symmetry seam in between, as shown in Fig. 1(a) and Table S1.

Steric effects, controlled by PES anisotropy, have long been recognized in adiabatic collisions.[43–45] In an activated reaction, the access of the reactive transition state is often facilitated by a cone of acceptance,[46] which influences not only the reactivity, but also product state distributions[47] and sometimes product branching.[48] It follows that stereodynamics could also have a significant impact on nonadiabatic dynamics, although such examples in collision processes are few and far between.[49, 50] The nonadiabatic quenching process discussed here serves as an excellent example for nonadiabatic barrierless scattering between molecular reactants.

Based on the stereodynamics described above, both the experimental and theoretical results can be rationalized. To begin with, we reconcile the aforementioned controversy concerning the branching ratio between the two quenching channels. In the work of Dempsey et al.,[25] the yield of the nonreactive channel (f_{R1b}) was measured directly; however, the yield for the reactive quenching channel (f_{R1a}) was derived with the assumption that the OH($A^2\Sigma^+$) radiative quenching is near completion, supported by the fast fluorescence decay time of OH($A^2\Sigma^+$) (165 ns) and the corresponding small yield.[29] While this assumption is reasonable, our quantum dynamics calculations revealed that the (in)elastic (R1c) channel is quite prominent due to the unique stereodynamics discussed above. Unfortunately, the existence of this channel was not considered in the branching ratio model of Dempsey et al.[25] Since the calculated absolute R1b fraction (f_{R1b}) is in good agreement with experiment, which further supports the accuracy of the DPEM, we speculate that the aforementioned assumption of neglecting the (in)elastic scattering channel might be flawed. Indeed, if we subtract the fraction of the R1c channel (f_{R1c}=0.772) from the experimental value for total nonreactive events (0.877), the fraction of the R1a channel (f_{R1a}) would be 0.105, which is very close to our calculated value of 0.100. Based on this argument, we propose a reinterpretation of the experimental results by including the (in)elastic yield, which leads to the conclusion that the reactive quenching is no longer the dominant channel. This conclusion is consistent with the earlier full-dimensional TSH results of Collins et al.[38] using their own DPEM.

An important caveat concerning the aforementioned branching ratio obtained from the quantum calculations is the lack of contributions of higher partial waves. While $N_{tot} > 0$ quantum scattering calculations are beyond the scope of this work, we have investigated this question using TSH with all accessible impact parameters (b_{max} = 5.5 Å or N_{max} = 35). The calculated fractions for the three channels at E_c=0.05 eV are as follows: 0.009 (R1a), 0.055 (R1b) and 0.93 (R1c). The increased dominance of the (in)elastic channel at large impact parameters is readily understood as the H_2-OH approach to the CI region is partially blocked by a centrifugal barrier while the (in)elastic channel is hardly affected. The inclusion of the higher partial waves in the entrance channel does not qualitatively change the conclusion.

The validity of the DPEM is further confirmed by the product state distribution in the nonreactive quenching channel. The OH rotational excitation can be attributed to the large anisotropy on the 1^2A and 2^2A state PESs, which exerts a strong torque on the departing OH fragment. This driving force exists not only in C_{2v}, as shown in Figure S5 and discussed in previous work,[29] but also in $C_{\infty v}$. This is illustrated in Fig. 6 where the potential along the coordinate is displayed at the collinear CI seam. The A' PES has larger anisotropy than the A" PES. On the other hand, the anisotropy along the angle is relatively small, leading to less rotational excitation of the H_2 product. The weak OH vibrational excitation stems from the fact that the equilibrium bond lengths of $OH(A^2\Sigma^+)$ (1.901 a.u.) and $OH(X^2\Pi)$ (1.825 a.u.) are similar. They are also quite close to that at the $C_{\infty v}$ MEX (1.820 a.u.). On the other hand, the H_2 vibrational excitation can be attributed to the stretched H-H bond at the $C_{\infty v}$ MEX. As shown in Table S1, the H-H distance at the MEX($C_{\infty v}$) is 1.776 a.u., which is significantly larger than its equilibrium value (1.406 a.u.). As shown in Movie S1, the wave functions on the 1^2A and 2^2A surfaces first shrink to a small H-H distance right after the nonadiabatic transitions and bounce by the potential wall at the small H-H value. Subsequently, the wave packet moves in a zigzag path in the exit channel, indicating vibrational excitation. Finally, the reproduction of the observed Λ-doublet propensity underscores the importance of out-of-plane dynamics and the CI seam between the two lowest electronic states leading to the $OH(X^2\Pi) + H_2$ products.

The exclusive population of the *ortho*-H_2 rotational states requires some additional explanation. The complete nuclear permutation and inversion (CNPI) group of H_3O is the D_{3h}. For discussion of the permutation symmetry of H_2 in the absence of H exchange with the OH group, the G_4 CNPI subgroup isomorphic to the C_{2v} point group is sufficient. In this subgroup, the electronic state correlating to the $OH(A^2\Sigma^+)$ reactant transforms as A_1, and states correlating to the $OH(X^2\Pi)$ products transform as B_1 and B_2. The character for the A_1 irrep under the permutation is + 1 (even), and that for the B_1 and B_2 irreps are − 1 (odd). Since the total symmetry (electronic + nuclear) is conserved, a *para*-H_2 (j = 0, even under permutation) reactant is expected to be transformed exclusively to *ortho* (odd j, odd under permutation) ones after nonadiabatic transitions.

4. Conclusions

The collisional quenching of $OH(A^2\Sigma^+)$ by H_2 has served as an important prototype for understanding nonadiabatic dynamics in bimolecular collisions. Although the underlying conical intersections have been identified for some time, the full-dimensional quantum characterization of the nonadiabatic dynamics has not been achieved until now. Using a highly accurate diabatic potential energy matrix that includes four lowest-lying electronic states, we report here for the first time full-dimensional quantum dynamics study of this prototypical nonadiabatic process involving four atoms and six coordinates. Our results revealed that the fate of $OH(A^2\Sigma^+) + H_2$ collision is largely determined by stereodynamics, namely the relative orientation between the two collisional partners. The quenching is made possible with the H_2-OH approach as H_2-HO collisions are ineffective in accessing the CI seam. Furthermore, nonadiabatic

transitions in the former orientation occur mostly near the collinear $C_{\infty v}$ CI seam, rather than the C_{2v} CI seam proposed in previous work.[29, 31] Most interestingly, the existence of a major (in)elastic channel, not included in the prior experimental analysis, suggests a reinterpretation of the experimental results that is consistent with the theoretical findings. This resolves a long-standing experiment-theory discrepancy concerning the reactive/nonreactive branching ratio. Finally, the OH($X^2\Pi$) and H_2 product state distributions were calculated and compared well with available experimental results. These results validate the accuracy of the recently developed diabatic potential energy matrix and shed valuable light on the complex nonadiabatic dynamics involved in the OH($A^2\Sigma^+$) quenching.

5. Methods

We employed a full-dimensional quantum wave packet method to study the collisional quenching of OH($A^2\Sigma^+$) by molecular hydrogen for zero total nuclear angular momentum (N_{tot}=0) on the recently constructed four-state DPEM.[40] As the details of the discretization, propagation, and product state projection are given in SI, we only provide a skeletal description here. The scattering calculations were performed using an exact kinetic energy operator in the diatom-diatom Jacobi coordinates (Fig. 1(c)). The fluxes to all three channels of R1 were computed from the wave packet initiated from the OH($A^2\Sigma^+$) + H_2 channel with both molecules in the ground ro-vibrational states and propagated in time using the split-operator method.[51] The OH and H_2 internal state distributions in both the ground and excited states were obtained in the asymptotic region, while the internal state of the H_2O product was not resolved. Absorbing potentials were placed in all three channels to enforce outgoing boundary conditions.

To validate the DPEM, scattering dynamics on the ground adiabatic state PES obtained from this DPEM was first carried out. The reaction probability agrees well with the most accurate ground-state PES of Chen et al.[52] (Figure S6 in SI). This DPEM is further validated by the nonadiabatic dynamics discussed above in comparison with available experimental results.

In addition to the quantum dynamics calculations, we have also carried out TSH calculations in the adiabatic representation using ANT,[53] in order to support mechanistic insights and to calculate the branching ratios. The details of the calculation are given in SI.

Declarations

Data Availability: All the data corresponding to the findings of this study are available from the corresponding author upon reasonable request.

Acknowledgements: The research at University of New Mexico and Johns Hopkins University is supported by the Department of Energy (DE-SC0015997). H.G. acknowledges a Humboldt Research Award from the Alexander von Humboldt Foundation. We thank useful discussions with Prof. Marsha Lester. The computation was performed at the Center for Advanced Research Computing at UNM.

Author contributions: The project was conceived by B.Z., D.R.Y., and H.G. The calculations were performed by B.Z. and S. H.. The results were analyzed by B.Z., S.H., C.L.M, U.M., D.R.Y., and H.G. The paper was written by B.Z. and H.G., with contributions from all authors.

Additional information: Supplementary information is available in the online version of the paper. Reprints and permissions information is available online at www.nature.com/reprints. Publisher's note: Springer Nature remains neutral with regard to jurisdictional claims in published maps and institutional affiliations. Correspondence and requests for materials should be addressed to B.Z. and H.G.

Competing financial interests: The authors declare no competing financial interests.

References

1. Born M, Huang K. *Dynamical Theory of Crystal Lattices*. Clarendon: Oxford, 1954.
2. Worth GA, Cederbaum LS. Beyond Born-Oppenheimer: Molecular dynamics through a conical intersection. *Annu Rev Phys Chem* 2004, **55**(1)**:** 127-158.
3. Jasper AW, Nangia S, Zhu C, Truhlar DG. Non-Born–Oppenheimer molecular dynamics. *Acc Chem Res* 2006, **39**(2)**:** 101-108.
4. Levine BG, Martínez TJ. Isomerization through conical intersections. *Annu Rev Phys Chem* 2007, **58:** 613-634.
5. Yarkony DR. Nonadiabatic quantum chemistry - past, present and future. *Chem Rev* 2011, **112**(1)**:** 481-498.
6. Domcke W, Yarkony DR. Role of conical intersections in molecular spectroscopy and photoinduced chemical dynamics. *Annu Rev Phys Chem* 2012, **63**(1)**:** 325-352.
7. Guo H, Yarkony DR. Accurate nonadiabatic dynamics. *Phys Chem Chem Phys* 2016, **18**(38)**:** 26335-26352.
8. Curchod BFE, Martínez TJ. Ab initio nonadiabatic quantum molecular dynamics. *Chem Rev* 2018, **118**(7)**:** 3305-3336.
9. Li J, Zhao B, Xie D, Guo H. Advances and new challenges to bimolecular reaction dynamics theory. *J Phys Chem Lett* 2020, **11**(20)**:** 8844-8860.
10. Juanes-Marcos JC, Althorpe SC, Wrede E. Theoretical study of geometric phase effects in the hydrogen-exchange reaction. *Science* 2005, **309:** 1227-1230.
11. Kendrick BK, Hazra J, Balakrishnan N. The geometric phase controls ultracold chemistry. *Nat Commun* 2015, **6:** 7918.
12. Yuan D, Guan Y, Chen W, Zhao H, Yu S, Luo C*, et al.* Observation of the geometric phase effect in the H + HD $\rightarrow$ H_2 + D reaction. *Science* 2018, **362**(6420)**:** 1289-1293.
13. Alexander MH, Manolopoulos DE, Werner H-J. An investigation of the F+H_2 reaction based on a full ab initio description of the open-shell character of the F(^{2}P) atom. *J Chem Phys* 2000, **113**(24)**:**

14. Alexander MH, Capecchi G, Werner H-J. Details and consequences of the nonadiabatic coupling in the Cl(^{2}P) + H_2 reaction. *Faraday Disc* 2004, **127**(0)**:** 59-72.
15. Che L, Ren Z, Wang X, Dong W, Dai D, Wang X*, et al.* Breakdown of the Born-Oppenheimer approximation in the F+ o-D_2 → DF + D reaction. *Science* 2007, **317**(5841)**:** 1061-1064.
16. Wang X, Dong W, Xiao C, Che L, Ren Z, Dai D*, et al.* The extent of non-Born-Oppenheimer coupling in the reaction of Cl(^{2}P) with para-H_2. *Science* 2008, **322**(5901)**:** 573-576.
17. Zhao B, Manthe U. Non-adiabatic transitions in the reaction of fluorine with methane. *J Chem Phys* 2020, **152**(23)**:** 231102.
18. An F, Chen J, Hu X, Guo H, Xie D. Nonadiabatic electronic energy transfer in the chemical oxygen–iodine laser: Powered by derivative coupling or spin–orbit coupling? *J Phys Chem Lett* 2020, **11**(12)**:** 4768-4773.
19. Yarkony DR. Diabolical conical intersections. *Rev Mod Phys* 1996, **68**(4)**:** 985-1013.
20. Domcke W, Yarkony DR, Köppel H (eds). *Conical Intersections: Theory, Computation, and Experiment*. World Scientific: Singapore, 2011.
21. Crosley DR. Rotational and translation effects in collisions of electronically excited diatomic hydrides. *J Phys Chem* 1989, **93**(17)**:** 6273-6282.
22. Lehman JH, Lester MI. Dynamical outcomes of quenching: Reflections on a conical intersection. *Annu Rev Phys Chem* 2014, **65:** 537-555.
23. Anderson DT, Todd MW, Lester MI. Reactive quenching of electronically excited OH radicals in collisions with molecular hydrogen. *J Chem Phys* 1999, **110**(23)**:** 11117-11120.
24. Todd MW, Anderson DT, Lester MI. Reactive quenching of OH A $^2\Sigma^+$ in collisions with molecular deuterium via nonadiabatic passage through a conical intersection. *J Phys Chem A* 2001, **105**(44)**:** 10031-10036.
25. Dempsey LP, Murray C, Lester MI. Product branching between reactive and nonreactive pathways in the collisional quenching of OH $A^2\Sigma^+$ radicals by H_2. *J Chem Phys* 2007, **127**(15)**:** 151101.
26. Lehman JH, Bertrand JL, Stephenson TA, Lester MI. Reactive quenching of OD $A^2\Sigma^+$ by H_2: Translational energy distributions for H- and D-atom product channels. *J Chem Phys* 2011, **135**(14)**:** 144303.
27. Ortiz-Suárez M, Witinski MF, Davis HF. Reactive quenching of OH($A^2\Sigma^+$) by D_2 studied using crossed molecular beams. *J Chem Phys* 2006, **124**(20)**:** 201106.
28. Dempsey LP, Murray C, Cleary PA, Lester MI. Electronic quenching of OH A^2S^+radicals in single collision events with H2 and D2: a comprehensive quantum state distribution of the OH X^2P products. *Phys Chem Chem Phys* 2008, **10**(10)**:** 1424-1432.
29. Cleary PA, Dempsey LP, Murray C, Lester MI, Kłos J, Alexander MH. Electronic quenching of OH $A^2\Sigma^+$ radicals in single collision events with molecular hydrogen: Quantum state distribution of the OH $X^2\Pi$ products. *J Chem Phys* 2007, **126**(20)**:** 204316.

30. Lehman JH, Dempsey LP, Lester MI, Fu B, Kamarchik E, Bowman JM. Collisional quenching of OD $A^2\Sigma^+$ by H_2: Experimental and theoretical studies of the state-resolved OD $X^2\Pi$ product distribution and branching fraction. *J Chem Phys* 2010, **133**(16)**:** 164307.
31. Lester MI, Loomis RA, Schwartz RL, Walch SP. Electronic quenching of OH $A^2\Sigma^+$ (v‘ = 0, 1) in complexes with hydrogen and nitrogen. *J Phys Chem A* 1997, **101:** 9195-9206.
32. Yarkony DR. Substituent effects and the noncrossing rule: The importance of reduced symmetry subspaces. I. The quenching of OH($A\,^2\Sigma^+$) by H_2. *J Chem Phys* 1999, **111**(15)**:** 6661-6664.
33. Hoffman BC, Yarkony DR. The role of conical intersections in the nonadiabatic quenching of OH($A^2\Sigma^+$) by molecular hydrogen. *J Chem Phys* 2000, **113**(22)**:** 10091-10099.
34. Dillon J, Yarkony DR. On the mechanism for the nonadiabatic reactive quenching of OH($A^2\Sigma^+$) by $H_2(^1\Sigma_g^+)$: The role of the 2^2A state. *J Chem Phys* 2013, **139**(6)**:** 064314.
35. Dillon J, Yarkony DR. Seams of conical intersections relevant to the quenching of OH($A^2\Sigma^+$) by collisions with H_2. *J Phys Chem A* 2013, **117**(32)**:** 7344-7355.
36. Fu B, Kamarchik E, Bowman JM. Quasiclassical trajectory study of the postquenching dynamics of OH A^2S^+ by H_2/D_2 on a global potential energy surface. *J Chem Phys* 2010, **133**(16)**:** 164306.
37. Zhang P-Y, Lu R-F, Chu T-S, Han K-L. Nonadiabatic quantum reactive scattering of the OH($A^2\,\Sigma^+$)+D_2. *J Chem Phys* 2010, **133**(17)**:** 174316.
38. Collins MA, Godsi O, Liu S, Zhang DH. An ab initio quasi-diabatic potential energy matrix for OH($^2\Sigma$) + H_2. *J Chem Phys* 2011, **135**(23)**:** 234307.
39. Shu Y, Kryven J, Sampaio de Oliveira-Filho AG, Zhang L, Song G-L, Li SL*, et al.* Direct diabatization and analytic representation of coupled potential energy surfaces and couplings for the reactive quenching of the excited $^2\Sigma^+$ state of OH by molecular hydrogen. *J Chem Phys* 2019, **151**(10)**:** 104311.
40. Malbon CL, Zhao B, Guo H, Yarkony DR. On the nonadiabatic collisional quenching of OH(A) by H_2: a four coupled quasi-diabatic state description. *Phys Chem Chem Phys* 2020, **22**(24)**:** 13516-13527.
41. Baer M. *Beyond Born-Oppenheimer: Electronic Nonadiabatic Coupling Terms and Conical Intersections*. Wiley: New Jersey, 2006.
42. Zhang P-Y, Lu R-F, Chu T-S, Han K-L. Quenching of OH($A^2\Sigma^+$) by H_2 through conical intersections: Highly excited products in nonreactive channel. *J Phys Chem A* 2010, **114**(24)**:** 6565-6568.
43. Stolte S. Reactive scattering studies on oriented molecules. *Ber Bunsenges Phys Chem* 1982, **86**(5)**:** 413-421.
44. Parker DH, Bernstein RB. Oriented molecule beams via the electrostatic hexapole: preparation, characterization and reactive scattering. *Annu Rev Phys Chem* 1989, **40:** 561-595.
45. Orr-Ewing AJ, Zare RN. Orientation and alignment of reaction products. *Annu Rev Phys Chem* 1994, **45**(1)**:** 315-366.

46. Levine RD. The chemical shape of molecules: an introduction to dynamic stereochemistry. *J Phys Chem* 1990, **94**(26)**:** 8872-8880.
47. Wang F, Lin J-S, Liu K. Steric control of the reaction of CH stretch-excited CHD_3 with chlorine atom. *Science* 2011, **331**(6019)**:** 900-903.
48. Lu D, Li J, Guo H. Stereodynamical control of product branching in multi-channel barrierless hydrogen abstraction of CH_3OH by F. *Chem Sci* 2019, **10**(34)**:** 7994-8001.
49. Falcinelli S, Vecchiocattivi F, Pirani F. Adiabatic and nonadiabatic effects in the transition states of state to state autoionization processes. *Phys Rev Lett* 2018, **121**(16)**:** 163403.
50. Zou J, Gordon SDS, Osterwalder A. Sub-Kelvin stereodynamics of the Ne($^3P_2$) + N_2 reaction. *Phys Rev Lett* 2019, **123**(13)**:** 133401.
51. Kosloff R. Time-dependent quantum-mechanical methods for molecular dynamics. *J Phys Chem* 1988, **92**(8)**:** 2087-2100.
52. Chen J, Xu X, Xu X, Zhang DH. A global potential energy surface for the H_2 + OH ↔ H_2O + H reaction using neural networks. *J Chem Phys* 2013, **138**(15)**:** 154301.
53. Zheng J, Li Z-H, Jasper AW, Bonhommeau DA, Valero R, Meana-Pañeda R*, et al.* ANT. University of Minnesota, Minneapolis; 2016.

Table

Table I. Branching fractions for the three channels of R1 at three different collision energies. The values in parenthesis were obtained from TSH calculations with zero impact parameters.

E_c (eV)	H+H_2O	H_2+OH(X^2P)			H_2+OH(A^2S^+)
		Total	OH(A′)	OH(A′′)	
0.05	0.098 (0.075)	0.123 (0.293)	0.086 -	0.037 -	0.772 (0.632)
0.16	0.111 (0.090)	0.282 (0.343)	0.186 -	0.096 -	0.606 (0.568)
0.30	0.187 (0.101)	0.339 (0.372)	0.219 -	0.119 -	0.476 (0.527)

Figures

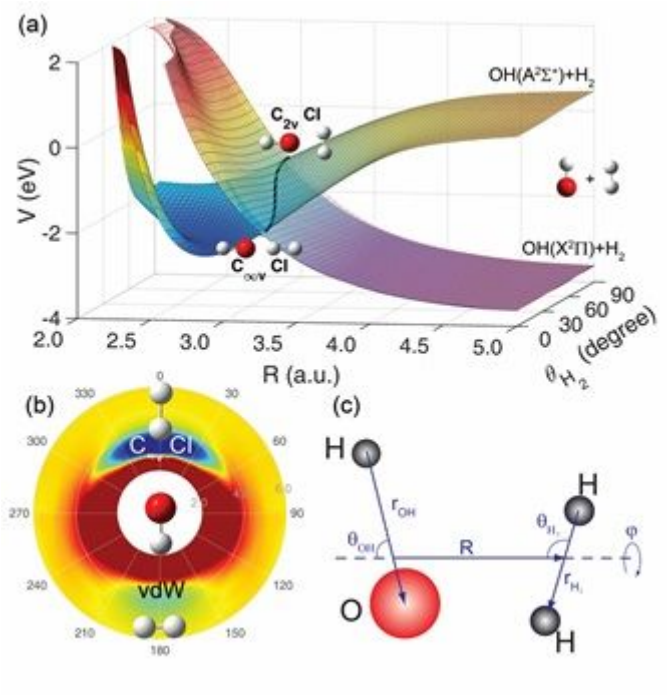

Figure 1

(a) 2D cuts of the three adiabatic PESs in the R and coordinates in the H2-OH orientation. The reference geometry is chosen at the C∞v MEX. (b) Polar plot of the adiabatic 32A surface with and as the radius and angle, respectively, with the remaining coordinates relaxed. The coordinates used in these plots and quantum calculations are defined in (c).

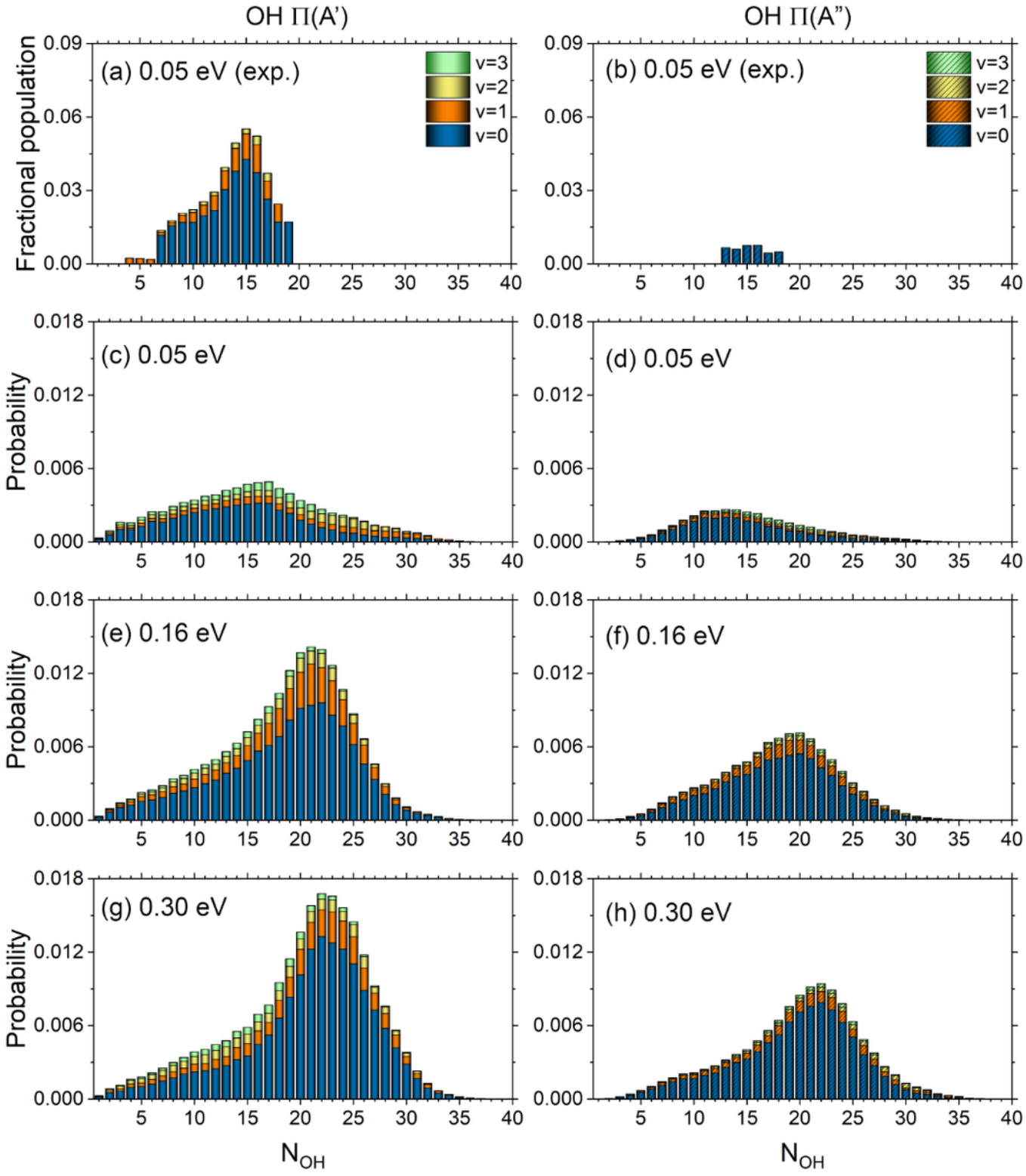

Figure 2

Experimental28 (a-b) and calculated (c-h) OH(X2) ro-vibrational state-resolved probabilities at three collision energies. Left and right columns are for OH(A') and OH(A"), respectively.

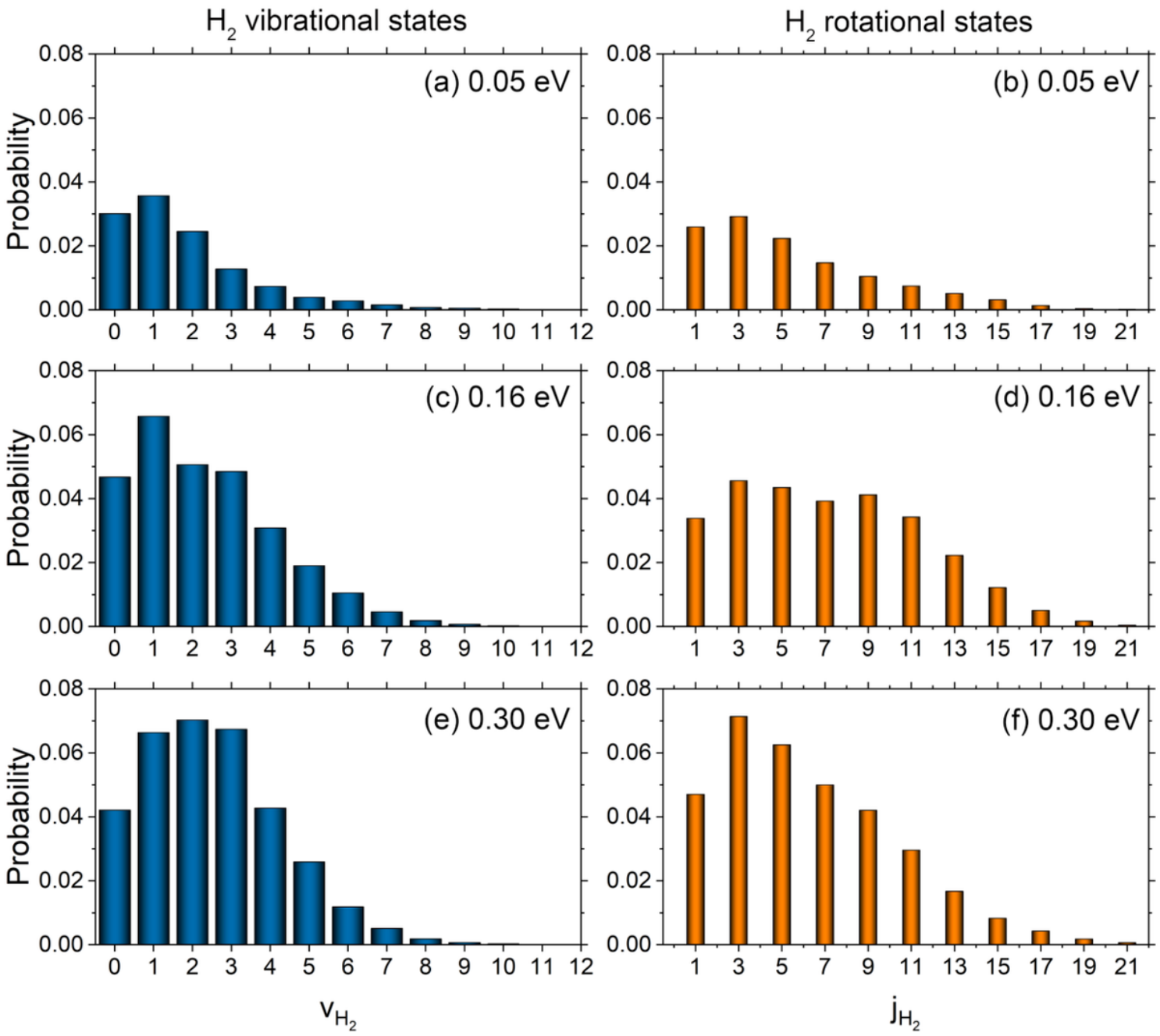

Figure 3

Calculated H2 vibrational and rotational state-resolved probabilities at three collision energies.

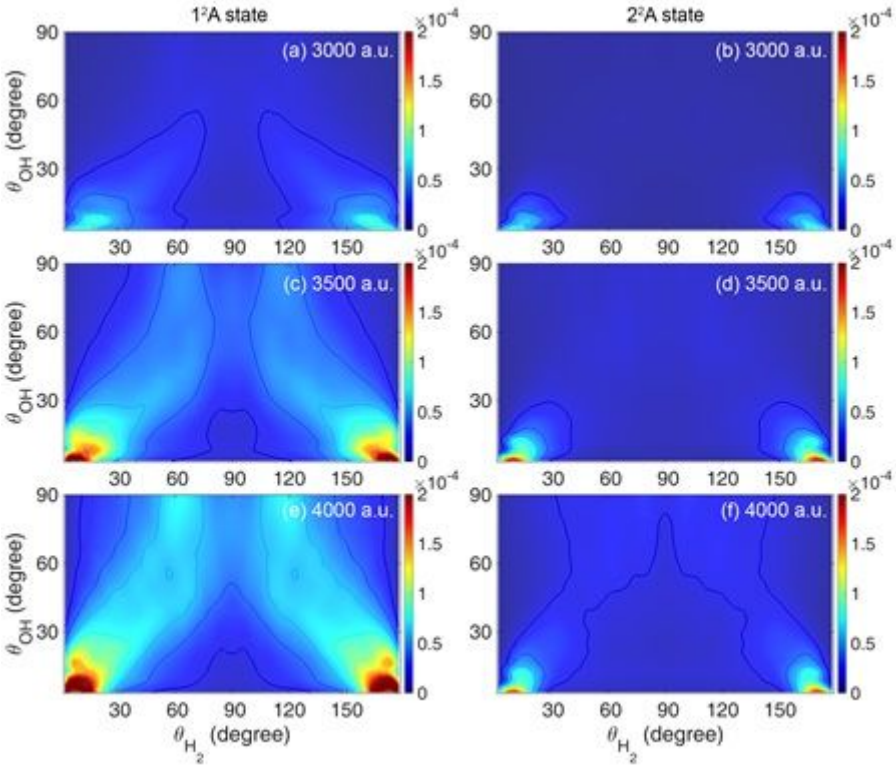

Figure 4

Plots of wave packet probability densities along and at three propagation times: Left and right columns are for the wave packet on the 12A and 22A states, respectively. The probability densities were obtained by integrating over the remaining four coordinates.

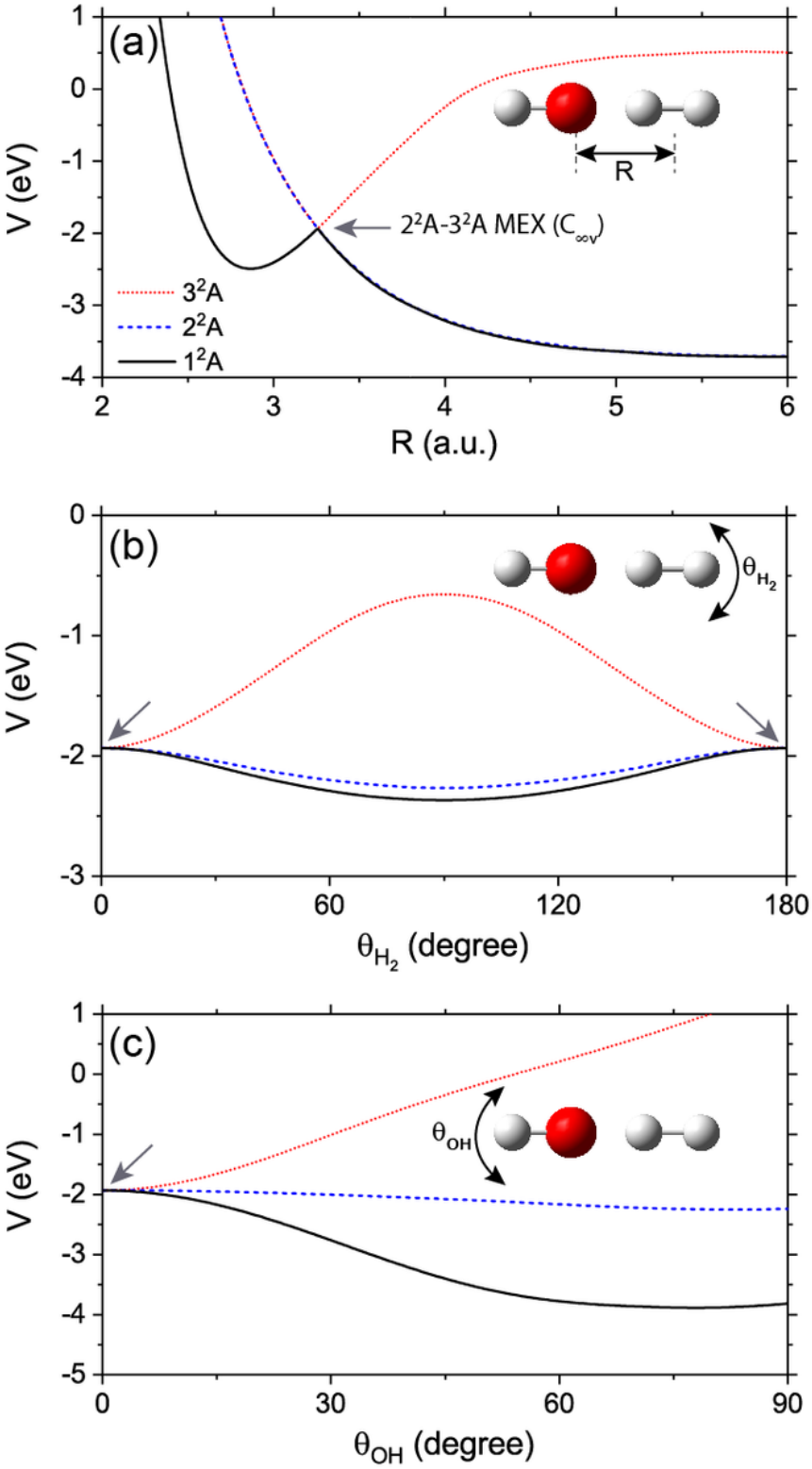

Figure 5

1D cuts of the three adiabatic surfaces in the H2-OH orientation. (a) dependence on the R coordinate. (b) dependence on the angle. (c) dependence on the angle. The reference geometry is taken at the C∞v MEX (see Table S1).

This is a list of supplementary files associated with this preprint. Click to download.

- MovieS1.mp4
- MovieS2.mp4
- MovieS3.mp4
- NonAdia.dynamicsofOHH2quenchSI20201216.docx
- TOCgraphic.jpg